Organic Process Research & Development

Article

pubs.acs.org/OPRD

Development of Continuous Anti-Solvent/Cooling Crystallization Process using Cascaded Mixed Suspension, Mixed Product Removal Crystallizers

Haitao Zhang, Justin Quon, Alejandro J. Alvarez,[†] James Evans, Allan S. Myerson, and Bernhardt Trout, II*

Department of Chemical Engineering, Massachusetts Institute of Technology, E19-502b, 77 Massachusetts Avenue, Cambridge, Massachusetts 02139, United States

[†]Department of Chemical Engineering, Tecnológico de Monterrey, Campus Monterrey, Av. Eugenio Garza Sada 2501, Monterrey, N.L. 64849, Mexico.

Supporting Information

ABSTRACT: This paper describes a two-stage mixed-suspension, mixed-product removal (MSMPR) continuous crystallization developed for a pharmaceutical intermediate which uses anti-solvent and cooling to generate supersaturation. The results indicate that the stage in which anti-solvent is added has a significant influence on the final crystal properties, while purity and yield were nearly identical. The population balance model was employed to determine growth and nucleation kinetics through parameter estimation. With the incorporation of measured equilibrium distribution coefficients, the model was used to optimize crystal purity and yield of the product with respect to operating temperature and residence time.

1. INTRODUCTION

Crystallization is an important separation and purification process for a broad diversity of solid product and intermediates in the bulk, fine chemicals, food, and pharmaceutical industries.[1] Manufacturing of almost all of the products based on fine chemicals, such as dyes, explosives, and photographic materials, include a crystallization step, and over 90% of all pharmaceutical products contain crystalline bioactive active pharmaceutical ingredients (API) and excipients. Crystallization processes in the pharmaceutical industry are usually designed to obtain crystals with controlled purity, size, shape, and polymorphic form in high yield. Normally, for the final pharmaceutical product, the control of crystal size, shape, and crystal form is crucial, as these properties can influence downstream operations such as filtration, drying, and milling as well as influence the physical and chemical properties such as dissolution rate and solubility. For the intermediates in the manufacturing process of pharmaceuticals, however, crystallization is normally employed as isolation and purification process. Controlled purity and yield of the product are the most important parameters. Knowledge of the process conditions required to fabricate crystals with controlled characteristics is critical during process development.[2,3]

Currently, pharmaceutical crystallizations are performed in batch mode using cooling, anti-solvent, or reactive crystallization techniques. Although the methodologies for developing these types of batch crystallization processes are reasonably well understood, there are still significant issues with batch-to-batch variability which can lead to substantial issues in the downstream processing of the isolated material.[4] Whilst a batch process may appear superficially simple, the underlying science and its control are highly complex, which can lead to problems in achieving consistent product specifications, e.g. size distribution, correct polymorphic form and morphology. These factors have a direct impact on downstream processes such as filtration, and ultimately on formulation into medicines and their performance.[5] Out-of-specification crystals are sometimes encountered, and therefore milling and recrystallization processes are other common unit operations in the pharmaceutical industry.[6]

There is tremendous potential to transform the entire industry by producing these products via continuous manufacturing. Moving to continuous processing has the potential for huge increases in efficiency, flexibility, and quality. Possible innovations include everything from continuous crystallization processes to novel separations and final finishing processes. Continuous reaction, workup, and crystallization have been identified as key elements in improving manufacture in the chemical and pharmaceutical industries.[7−10]

The center for continuous manufacturing focuses on the development these new technologies that will allow continuous pharmaceutical manufacturing. As part of the whole project, our team is exploring the use of various types of continuous crystallization for pharmaceutical intermediates and final products of APIs. Issues related to purity, polymorphism, crystal size distribution, crystal shape, scale-up, and recycling are being studied.

The most common types of continuous crystallizers are continuous mixed-suspension, mixed-product removal (MSMPR) and plug-flow reactor (PFR) crystallizers. Models for both types developed by Randolph and Larson[4] have been used extensively by various investigators for the simultaneous determination of nucleation and growth kinetics in crystallization systems.[6,11,12]

Special Issue: Continuous Processes 2012

Received: October 13, 2011
Published: March 14, 2012

dx.doi.org/10.1021/op2002886 | *Org. Process Res. Dev.* 2012, 16, 915−924

Both MSMPR and PFR crystallizers have their advantages, and the choice of whether to use a MSMPR or a PFR system is primarily driven by the kinetics of the process, with MSMPR generally being preferred for low conversions and long residence times and the PFR being preferred for higher conversions with short residence times. A secondary factor favoring the utilization of the MSMPR approach is the fact that it is relatively simple to convert existing batch capacity to continuous capacity.[7] For the system being studied here, MSMPR crystallizers were found to be more appropriate. A series of MSMPR crystallizers in cascade offers a viable alternative that not only narrows the CSD but also offers other improvements including flexible operation of temperature regimes, the possibility of using larger cooling surfaces, and economies of energy consumption.[5] This paper investigates experimentally and through population balance modeling the cascaded MSMPR multistage crystallization system developed to perform a continuous anti-solvent/cooling crystallization.

The major issues covered in this paper are the following:

- development of the continuous crystallization system
- results of continuous crystallization experiments
- experimental determination of distribution coefficients
- development of multistage model to predict purity and yield

2. EXPERIMENTAL SECTION

2.1. Materials. Compound A is very soluble in alcohols including methanol, ethanol, and isopropanol, sparingly soluble in ethyl acetate (EtOAc), butyl acetate, propyl acetate, and toluene, and is nearly insoluble in heptane and water. Precursor 1, the main impurity in the crystallization mother liquor, is very soluble in most of the organic solvents and nearly insoluble in water.

2.2. Apparatus. Multistage continuous crystallization experiments were carried out in a self-assembled multistage crystallization system. Each stage was operated as an MSMPR crystallizer. The experimental system consisted of two 50-mL (mL) glass-jacketed crystallizers with independent temperature control and overhead mechanical stirring. Feed solution containing Compound A was continuously pumped into the first crystallizer using a peristaltic pump (flow rate range 0.006–600 mL/min, MasterFlex, provided by Cole-Parmer corporation). In this study, two different configurations were studied. In the first configuration, Configuration A, supersaturation was generated in the first vessel using cooling, and supersaturation was generated in the second vessel using both cooling and anti-solvent addition. For Configuration B, supersaturation was generated in the first vessel using both anti-solvent and cooling, and the second vessel was cooled even further. Schematics of the experimental setup can be seen in Figure 1. The suspension that was generated in the first crystallizer was transferred to the second stage using a peristaltic pump. The temperature of both vessels was controlled ±0.1 °C with a NESLAB RTE Refrigerated Bath Circulator.

The concentrations of Compound A and Precursor 1 in the feed material and mother liquor were measured by high performance liquid chromatography (HPLC). Mother liquor samples were taken by filtering slurry samples from each vessel using PTFE syringe filter with 0.2-μL pore size. An HPLC instrument (Agilent Technologies 1200 series) with a Nucleosil 100-3 C18 (4.0 mm × 125 mm, 3 μm) column was used to measure at 230 nm, using an Agilent 1200 series UV detector, with the following measuring conditions: flow rate of 1.0 mL/min, 20-μL injection volume, and 50 °C operating temperature.

Chord length distribution (CLD) of the solid product was measured with focused beam reflectance measurement (FBRM).[13,14] The FBRM device was a Lasentec S400 probe from Mettler Toledo, with a measurement range from 785 nm to 1000 μm. X-ray diffraction patterns were recorded with a PANalytical X'Pert PRO Theta/Theta Powder X-ray Diffraction System with a Cu tube and X'Celerator high-speed detector. Differential scanning calorimetry (DSC) measurements were performed using a Q5000 DSC from TA Instruments. Crystal morphology was observed by a Zeiss Axiovert 200 optical microscope in transmission mode with a differential interference contrast (DIC) polarizer and magnification range from 5× to 50×.

2.3. Procedure. Anti-solvent/cooling continuous crystallization experiments for Compound A were performed using the continuous crystallization apparatus described in Figure 1. The feed solution consisted of EtOAc with 13% (m/m) Compound A at room temperature, 2% (m/m) Precursor 1, and 1% (m/m) impurities that were generated in the synthesis of Compound A. The feed solution was directly pumped into the first crystallizer at a flow rate 0.125 mL/min. The working volume of the first stage was 30 mL, and the residence time of each stage was set to 4 h. The slurry in the first crystallizer was then pumped into the second crystallizer. Concurrently, an anti-solvent stream of heptane was added to the vessel. The heptane flow rate was set such that it would comprise 25% (m/m) of the solvent mass (0.036 mL/min). The temperatures of Stages 1 and 2 were −5 and −10 °C, respectively. The duration

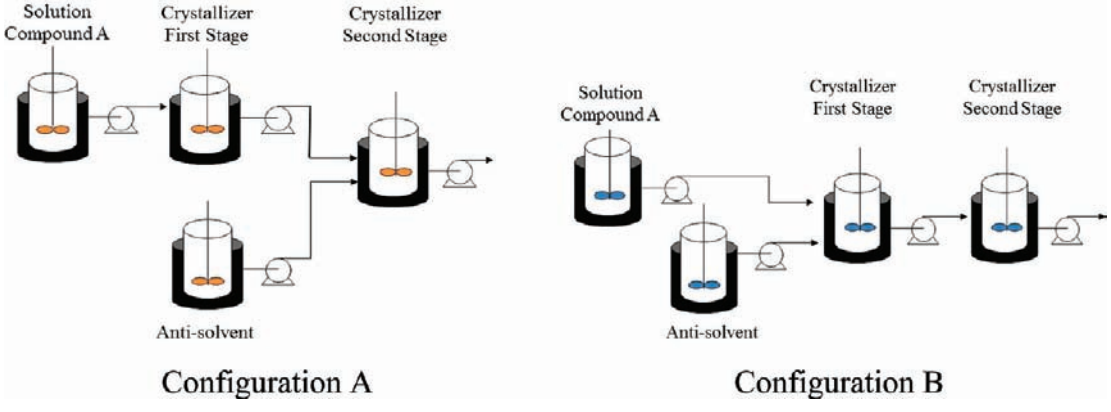

Figure 1. Schematic diagram of continuous crystallization apparatus.

dx.doi.org/10.1021/op2002886 | Org. Process Res. Dev. 2012, 16, 915–924

of the experiment was 33 h (four total residence times). The concentration of the mother liquor and the chord length distribution were both monitored over time. Once the signals leveled out, steady state was reached.

After the system was run for four residence times, a sample (approximately 5 mL) of the slurry was withdrawn from each stage, and concentration measurements were performed as described previously. The crystals in each stage were also analyzed for purity (HPLC), crystal structure (PXRD), crystal morphology (optical microscopy), and chord length distribution (FBRM).

3. RESULTS AND DISCUSSIONS

3.1. Development of the Continuous Crystallization System. *Influence of Water on the Crystallization Process of Compound A.* The feed solution to the crystallization consisted primarily of Compound A and Precursor 1 in ethyl acetate. Crystallization experiments using pure ethyl acetate, Compound A, and Precursor 1 to form the starting solution resulted in a yield of 92% Compound A recovered with greater than 98% purity. Crystallization using feed material from an actual reaction (as opposed to using pure materials) gave a yield of 62% with significantly lower purity.

A review of the reaction and workup steps suggested that because of an upstream liquid–liquid separation step, nearly 5% water was being entrained in the organic stream. The effect of water on the solubility of Compound A can be seen in Figure 2.

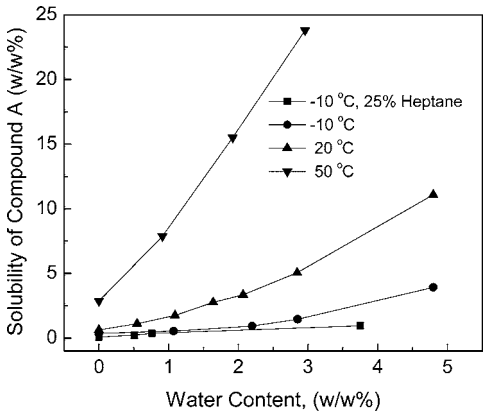

Figure 2. Compound A solubility versus water content in the organic phase at different temperatures and solvent compositions.

The presence of water significantly increased the solubility of Compound A at all measured temperatures. This was unexpected, as Compound A has low solubility in both pure ethyl acetate and pure water, but a higher solubility in the mixed solvent.

A secondary solvent screen was undertaken to identify a suitable anti-solvent to improve the crystallization yield. Heptane was identified as a promising choice for the anti-solvent system. With the addtion of heptane, the solubility of Compound A was significantly reduced. From Figure 2, it can be seen that the addition of 25% heptane reduced the solubility of Compound A at all water cotent levels. At 3.5% water, adding 25% heptane reduced the solubility of Compound A to below 0.9%, compared to around 2.5% for the solution without heptane. The solubility of Compound A became stable with respect to increasing heptane content at 25% heptane solvent content. In consideration of the working volume increase and the Compound A concentration decrease with the addition of heptane, the heptane content was set at 25 (m/m) % of the total solvent.

On the basis of the above results, we employed a continuous anti-solvent + cooling procedure for the Compound A crystallization with the temperature of the first crystallizer set at −5 °C and the second stage set at −10 °C.

Influence of Anti-Solvent on Crystal Properties. To investigate the influence of anti-solvent on crystal properties, X-ray diffraction patterns of Compound A crystallized with varying heptane concentrations were measured, and the results are shown in Figure 3. As the concentration of the anti-solvent

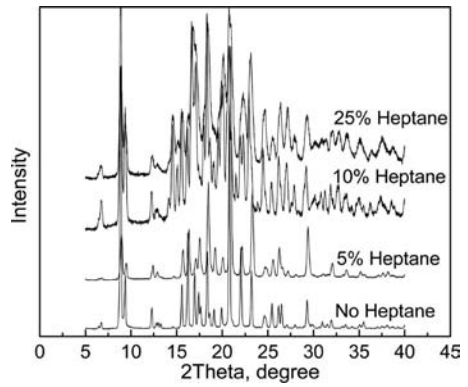

Figure 3. X-ray diffraction of Compound A crystallized in EtOAc with different heptane content.

was increased, the level of supersaturation also increased. This leads to a higher rate of nucleation and thus more fines and amorphous material in the final product. These are identified by peak broadening and a raised baseline of the diffraction patterns. From an optical microscope picture as shown in Figure 4, it can be seen there are some large agglomerates in the crystals generated using 25% anti-solvent.

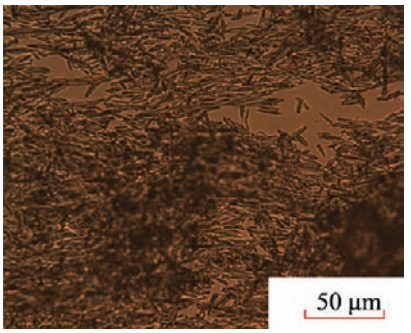

Figure 4. Microscope images of Compound A crystallized in batch with 25% heptane.

During the process development, it was not initially clear whether adding the anti-solvent in the first or the second vessel was a better option due to the unknown kinetic information. To answer which option will be better, the effect of the anti-solvent addition on the crystal properties was determined.

The XRD patterns and optical microscope pictures for crystals generated with anti-solvent feeding in the first stage can be seen in Figures 5 and 6, respectively. Figures 7 and 8 contain XRD and optical microscope pictures for crystals generated with anti-solvent added into the second vessel.

dx.doi.org/10.1021/op2002886 | Org. Process Res. Dev. 2012, 16, 915–924

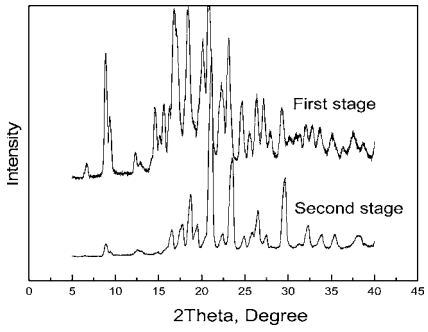

Figure 5. X-ray diffraction of Compound A crystallized in ethyl acetate + 25% heptane from the continuous crystallization process with anti-solvent feeding at the first stage.

The crystals generated with anti-solvent feeding at the second stage have better crystallinity compared to those generated with anti-solvent feeding at the first stage. Comparing the X-ray patterns in Figures 5 and 7, the crystals from the continuous process with anti-solvent feeding at the second stage have a much stronger baseline with much sharper and narrower peaks. DSC curves shown in Figure 9 help demonstrate this crystallinity result. As shown in the DSC curves, for the product generated by adding anti-solvent in second stage, the melting peak is sharper and narrower, and its enthalpy of fusion is higher and thus more crystalline. By adding anti-solvent in the second stage, the supersaturation in the first stage vessel is significantly decreased, and the entire process was operated at lower supersaturation level. From the optical microscope pictures, the crystals generated with anti-solvent added in the first vessel are much more agglomerated. Crystals generated with anti-solvent added to the second vessel are more suitable for downstream processing because they allow for an easier downstream filtration step.

3.2. Evolution of Continuous Crystallization Process. The temperature, yield of crystallization, and the CLD of the crystals in the two stages were tracked over the duration of crystallization process to monitor the process state to confirm that steady state was reached.

As shown in Figure 10, the temperature in each stabilized after 1−2 residence times. Initially, no temperature was recorded until the level of slurry reached the temperature probes.

The concentration of Compound A in the mother liquor and the CLD of both stages were tracked over the duration of the crystallization process. As shown in Figure 11, the yield stabilized after 3 residence times. From Figures 12 and 13, the CLD also stabilized after 3 residence times.

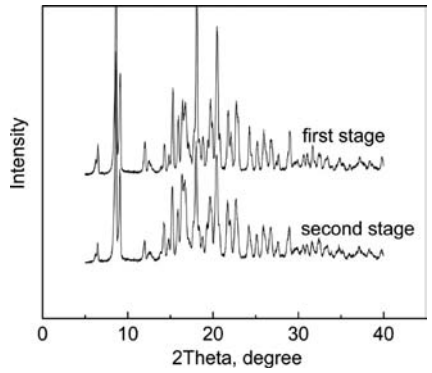

Figure 7. X-ray diffraction of Compound A crystallized in EtOAc + 25% heptane from the continuous crystallization process with anti-solvent feeding at the second stage.

As can be seen from Figures 11−13, after 3−4 residence times, the variables monitored were consistent and indicate that the steady state was reached.

To determine if there was significant classification in the crystallizers, samples were taken at different locations in the second stage, including the top of the crystallizer, the bulk slurry, and the bottom of the crystallizer. No significant difference was observed as shown in the microscope images in Figure 14.

3.3. Experiments to Determine Distribution Coefficients. A sequence of anti-solvent and cooling crystallization experiments of Compound A in EtOAc was carried out to determine equilibrium distribution coefficients of the impurities. Heptane was added to a saturated solution of Compound A in EtOAc at 25 °C in increments of 5% heptane by mass up to a total of 25% heptane. The solution was then cooled to −10 °C in increments of 5 °C. After each step, the crystallized solids were separated by filtration and dried overnight. Samples of solids and mother liquor were analyzed by HPLC to determine distribution coefficients.

When impurities incorporate at small level into the crystal, the incorporation can be characterized by a distribution coefficient which is defined as the ratio of impurity concentrations to the host compound concentration in the solid phase divided by that ratio in the liquid phase. The followed equation defines the distribution coefficient.[15]

$$\text{distribution coeff.} = \frac{(C_{\text{imp}}/C_{\text{Compound A}})_{\text{solid}}}{(C_{\text{imp}}/C_{\text{Compound A}})_{\text{liquid}}} \quad (1)$$

where C_{imp} is the concentration of impurity and $C_{\text{Compound A}}$ is the concentration of the API.

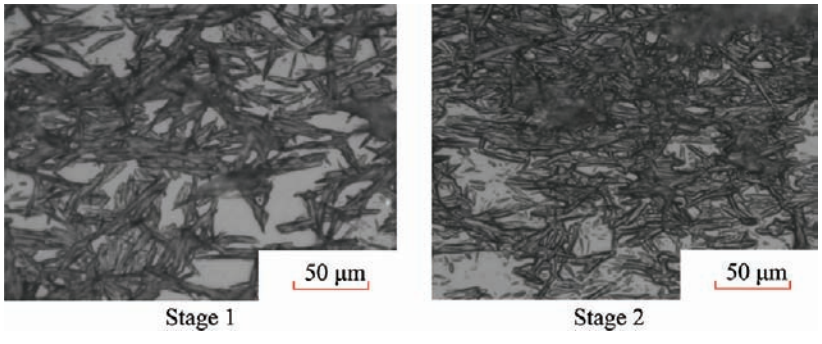

Figure 6. Microscope images of Compound A in the two stages from the continuous crystallization process with anti-solvent feeding at the first stage.

dx.doi.org/10.1021/op2002886 | Org. Process Res. Dev. 2012, 16, 915−924

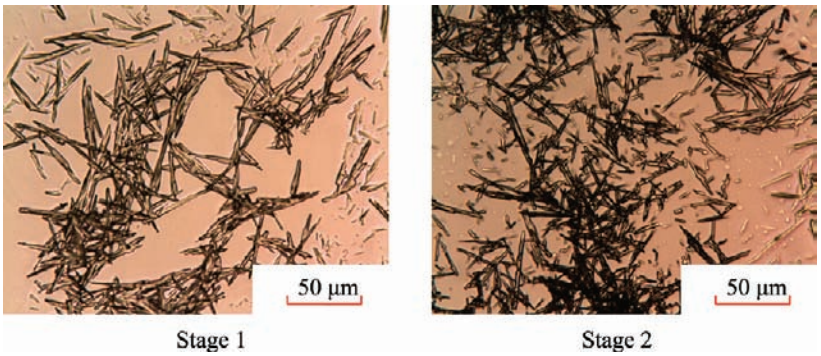

Figure 8. Microscope images of Compound A in the two stages from the continuous crystallization process with anti-solvent feeding at the second stage.

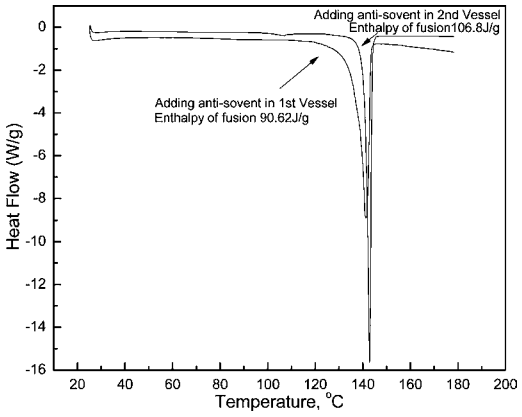

Figure 9. Comparison of DSC curves of the final products of compound A with two approaches.

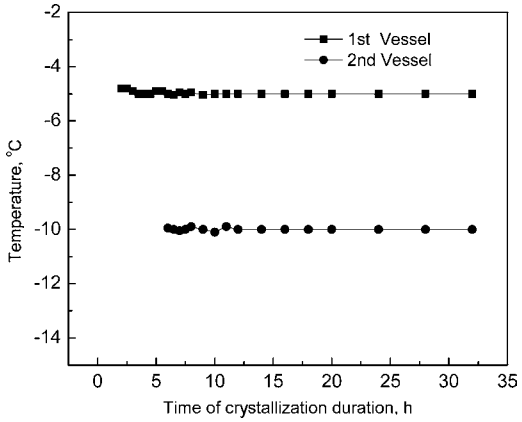

Figure 10. Temperature versus time in the two stages.

Distribution coefficients for Compound A impurities were calculated by applying eq 1 to data obtained experimentally. A plot of the distribution coefficient as a function of the purity of the initial solution is shown in Figure 15. This information was then used to model the continuous crystallization process and determine the effect of process conditions on purity and yield.

The variation of the distribution coefficient can be attributed to a couple of reasons. First, the current crystallization process is a combined cooling/anti-solvent process. The variation of impurity affinity with the solvent plays a key role for the variation of the impurity distribution level. As shown in Figure 15, there is a big variation for the distribution coefficient over the impurity level while changing the solvent system from cooling crystallization to

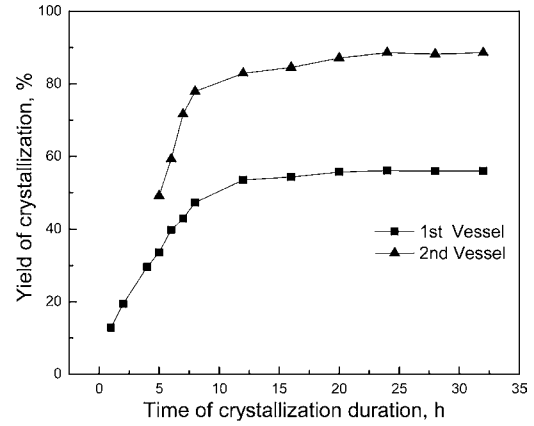

Figure 11. Yield evolution in the two stages during the time of crystallization duration in the two stages.

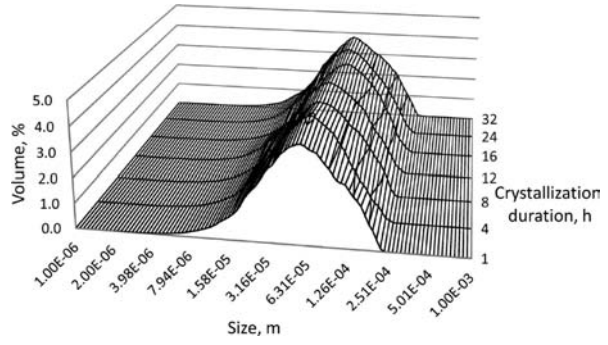

Figure 12. CLD evolution in the first stage.

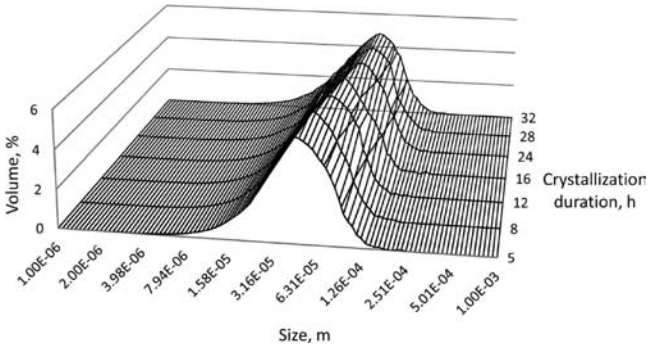

Figure 13. CLD evolution in the second stage.

an anti-solvent crystallization. Changing the solvent composition and properties leads to the variation of the impurity activity in the

dx.doi.org/10.1021/op2002886 | Org. Process Res. Dev. 2012, 16, 915–924

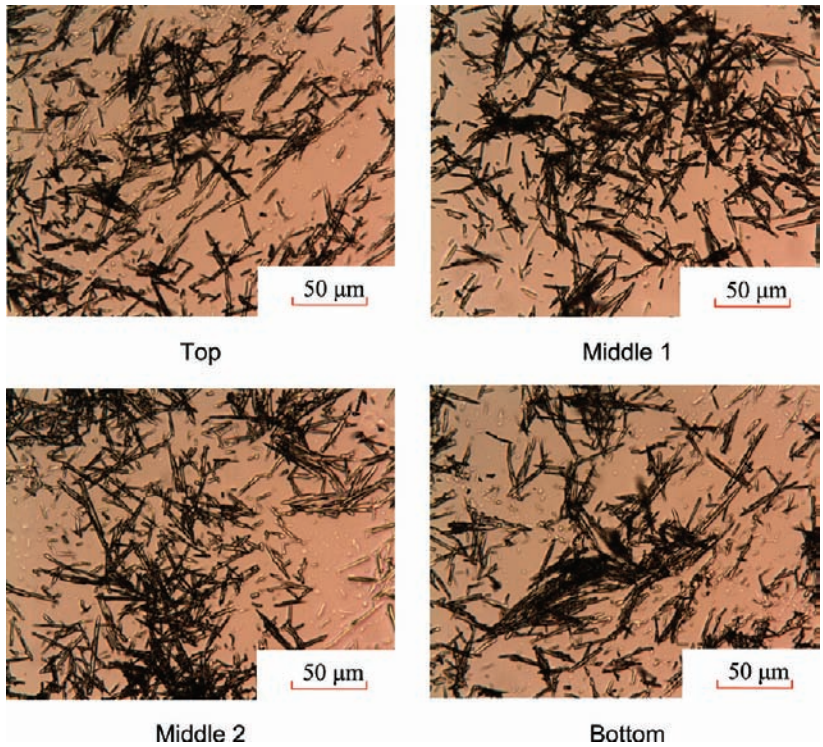

Figure 14. Microscope images of the crystals taken at different locations in the second vessel.

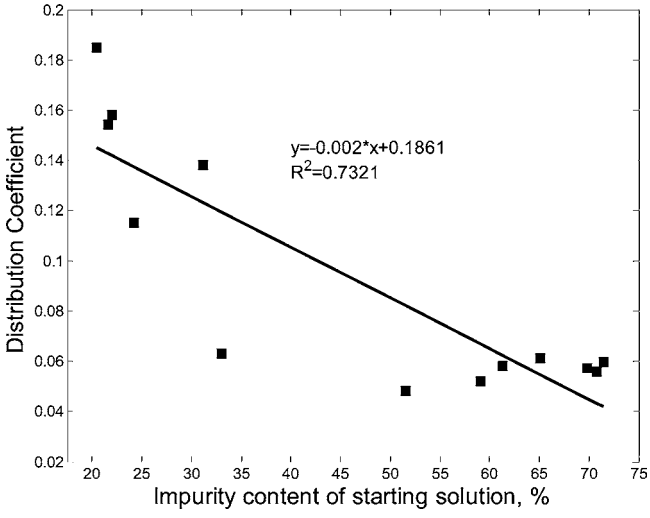

Figure 15. Distribution Coefficients as a function of the purity of the starting solution.

solution and the affinity with the solvents and hence induces variation in the impurity distribution level. Also the temperature change in the cooling process can cause the variation of the impurity-dissolving performance in the solvent and hence induces the variation of the impurity distribution level. Second, during the experimental process, we gave same reaction time for each step to achieve equilibrium. However, there are still some deviations between the experimental state and the equilibrium state. Thus, it is possible that some points in Figure 15 show a big deviation. Finally, the different mixing profiles and working volume can be considered to generate the experimental errors.

3.4. Mathematical Model of Cascaded Multistage Crystallization System. Because this process was developed for an intermediate crystallization, the most important parameters are process yield and crystal purity. Properties such as crystallinity and size distribution are not as important because the intermediate product will be redissolved in further downstream processing. A model relating nucleation and crystal growth kinetics to operating variables is necessary to evaluate the effect of operating conditions on the purity of the crystal and the process yield. A model of the continuous crystallization process based on the simultaneous solution of the population balance equation (PBE) and mass balance equation has been developed. The purpose of the model is to predict the crystal purity, yield, and size distribution of the crystals obtained in the multistage cascaded continuous crystallization system.[1,4,16−18]

FBRM was employed as a tool to measure our samples despite its limitations especially for nonspherical crystals. FBRM is a laser backscattering particle size analyzer. A laser is shined into the samples, and as the beam crosses the surface of a particle or particle structure, light from the beam is backscattered into a probe. The duration of each reflection is multiplied by the velocity of the scanning beam, resulting in a chord length. Typically, many thousands of chord lengths are measured per second, with the numbers of counts dependent on the concentration of solids present in the suspension. The number of chords reported and their measured length will be intimately related to the measuring principles (including the particle diameter, concentration and shapes, optical properties of the materials) and the flow conditions near the probe tip. Spherical particles will give far more chord lengths close to the average particle size than rodlike or needlelike crystals, for which the dominant chord length may be closer to the minor axis length.[21] This limitation may cause deviation of the measured CLD data from the actual size distribution. For example, the acicular crystals can grow significantly in the axial direction, but FBRM is less sensitive to growth in the axial direction.

However, prior research has attempted to relate CLD to the PSD. In a number of cases,[19−25] it has been demonstrated that

there is a good agreement between the normalized chord length data and the measured particle size distribution. Thus, it allowed for a translation of the CLD to the corresponding PSD at least under a few of the assumptions of the particle shape. Togkalidou[19] has demonstrated it is an alternative approach applicable in the early-stage design of pharmaceutical crystallization processes to use the low-order moments of the CLD directly, without first converting the CLD measurement to a PSD estimate. As a result, it is possible to extract sufficient information to enable us to estimate the kinetic performance/parameters of our process by FBRM, and it is also demonstrated by the results in this work.

The model is built on the basis of the theory of population balance, which is based on the concept of continuous mixed-suspension, mixed-product removal (MSMPR) crystallizers developed by Randolph and Larson,[4] and its power of the population balance for analysis of crystallizers is demonstrated by its application to a continuous crystallizer.[4,5,9] The model is a useful tool to study the purity and yield since equilibrium distribution coefficients were measured and included in the model. The model equations used can be seen in Supporting Information (SI). In this model, nucleation and growth rate kinetic parameters were estimated from experimentally determined chord length distributions using nonlinear optimization.

3.4.1. Parameter Estimation. As described in the previous section, the MSMPR model can be used to estimate the nucleation and crystal growth rate kinetic parameters by solving the optimization problem defined in eq 13 in the SI. This approach was used to obtain kinetics from the continuous crystallization experiment of Compound A in EtOAc–heptane. There are a couple of assumptions that are incorporated in the current model including (1) the nucleus size is small, (2) the surface nucleation, agglomeration, and attrition/breakage are negligible. Process parameters for the experiments can be seen in Table 1.

Table 1. Process conditions for estimation of nucleation and crystal growth kinetic parameters

condition	value	units
volume stage 1, $V1$	30	mL
volume stage 2, $V2$	41	mL
flow rate stage 1, $Q1$	0.125	mL/min
flow rate stage 2, $Q2$	0.174	mL/min
temperature stage 1, $T1$	−5	°C
temperature stage 2, $T2$	−10	°C
solubility at $T1$	0.0318	kg/kg
solubility at $T2$	0.0089	kg/kg
concentration of API, C_o	95.2	kg/m^3
density of crystal	1200	kg/m^3
density of solvent	897	kg/m^3
density of anti-solvent	684	kg/m^3

Table 2 shows the volume-based mean crystal size obtained in stages 1 and 2 as well as the supersaturation in each stage.

Table 2. Mean crystal size (volume-based) in stages 1 and 2 in the continuous crystallization experiment for Compound A

stage	temperature (°C)	residence time (min)	supersaturation	mean size (μm)
1	−5	240	0.35	71.69
2	−10	240	0.29	71.77

It was observed that the mean size of Compound A crystals in each stage was not significantly different. This is because the anti-solvent was introduced in the second stage, and thus the supersaturation was kept at similar level in both stages. At the same time, a high supersaturation level in stage one was avoided, and the nucleation rate and the crystal growth rate in both of the two stages were kept at the suitable level in the entire process, and the final product with higher crystallinity and better crystal morphology was generated (Figures 7 and 8).

The results from the two stages were included in the optimization, and the difference between calculated and experimental crystal size distribution was minimized. To obtain an efficient optimization and accelerate convergence, the parameters k_{g0}, k_{g1}, and k_b were scaled nonlinearly, using $\ln(k_{g0})$, $\ln(k_{g1})$, and $\ln(k_b)$, respectively. The results of the parameter estimation are shown in Table 3. A comparison between the calculated and experimental chord length distributions can be seen in Figure 16.

Table 3. Estimated nucleation and crystal growth kinetic parameters for Compound A continuous crystallization with two-stage cascaded MSMPR crystallization system

parameter	value	units
k_g @ −5 °C	2.33×10^{-7}	m/min
k_g @ −10 °C	9.86×10^{-8}	m/min
k_{g0}	9.81×10^{12}	m/min
k_{g1}	12116	J/mol
k_b	6.92×10^{11}	#/m^3·min
g	1.09	dimensionless
b	3.99	dimensionless

3.4.2. Model Validation. In order to test the validity of the model, the experiments were rerun with different parameters. The previously calculated parameters were then used to simulate the effects of changing these experimental parameters, and the results were then compared. The temperature of the first stage was changed to 0 °C, and samples were taken in the two stages at steady state to measure the CLD by FBRM. As shown in Figure 17, the model results agree reasonably with the experimental size distribution. Linear kinetic order for crystal growth and quadratic kinetic order for nucleation are both physically realistic results. The differences between the model and the experimental data can be explained in part by the fact that Compound A crystals have a needlelike morphology (Figure 8). One assumption of the model is that the crystals have perfectly spherical morphology, and this difference is known to impact on the accuracy of the model.[19,26,27] With a needlelike morphology the needle width has a greater probability than the needle length of being measured by the scanning laser. For the FBRM chord length distributions, an increase in number of small chord lengths does not necessarily imply secondary nucleation, but can also be indicative of crystal growth. An increase in needle length will lead to an increase in small chord lengths counted over time.

In addition to the spherical crystal assumption, there are a number of other assumptions involved in the population balance equation which will give rise to differences between the experimental and predicted crystal size distributions. It is assumed that the product CLD is the same as that found within the crystallizer, i.e. there is no classification of the particles in the crystallizer taking place. This is the standard assumption used in reaction engineering to define a well-mixed reaction vessel. This might not be the case if there is imperfect mixing or dead zones in the vessel. Second, it is assumed that particles are formed only by nucleation and increase in size only through growth and that the processes of breakage, attrition, and agglomeration are negligible.

dx.doi.org/10.1021/op2002886 | Org. Process Res. Dev. 2012, 16, 915–924

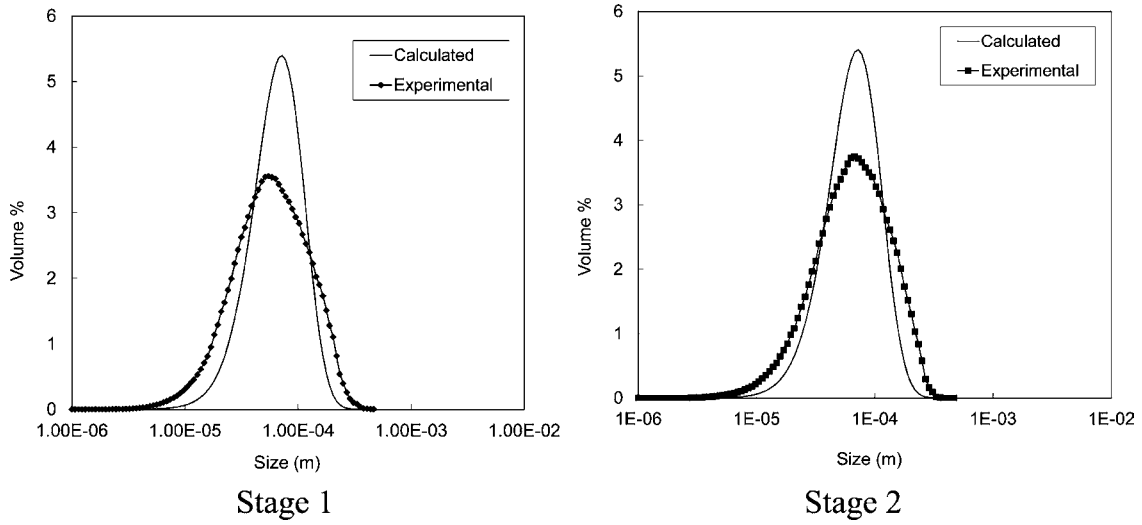

Figure 16. Predicted and experimental CLD for Compound A continuous crystallization.

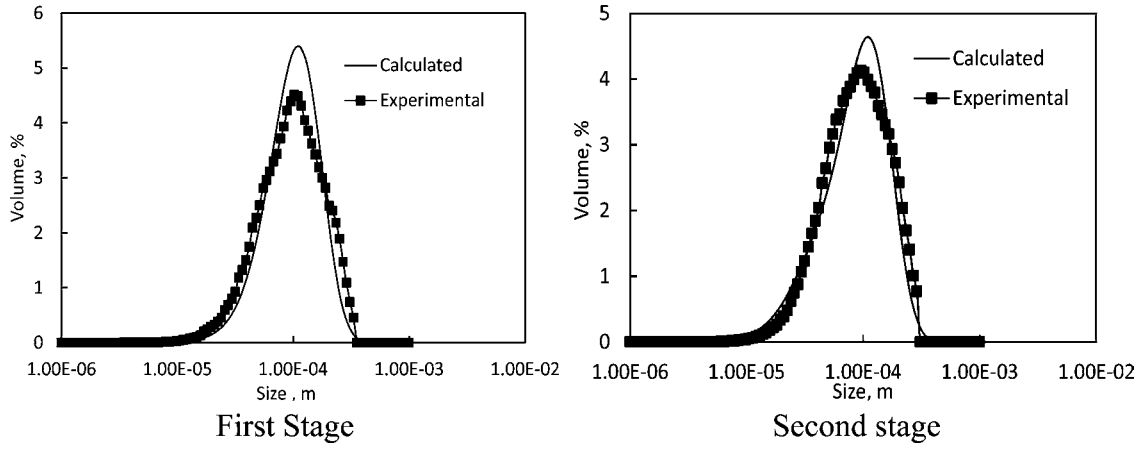

Figure 17. Predicted and experimental CLD for Compound A continuous crystallization for model validation.

In the real system, agglomeration and the breakage of the crystals are inevitable and can be a significant factor especially for systems with needle morphology. Finally, because the crystals are needles, the assumption that shape factors for particles are not a function of size may not be completely accurate. Unlike spheres, a needle cannot be described with a single characteristic size, unless the aspect ratios for all needles are equivalent. Breakdowns in these assumptions provide additional deviations when comparing the model with the experimental data.

3.5. Effect of Process Conditions on Crystal Purity and Yield. The multistage MSMPR model was used to evaluate the effect of operating conditions on the purity of the crystal and the process yield in the continuous crystallization process of Compound A. The influence of the temperature and residence time of both of the two stages on the crystal purity and the process yield are evaluated. The effect of the temperature of each stage on the product yield purity can be seen in Figure 18. For comparison, in the batch experiments at −5 °C, and −10 °C, the purity of the crystals was 89.60% and 88.48%, respectively.

Changing the temperature of each stage has a significant effect on the process yield. By varying the temperature by 15 °C from the actual chosen operating temperatures, the yield decreased from 89.8% to 85.7%. This is because the solubility of Compound A increases with increasing temperature.

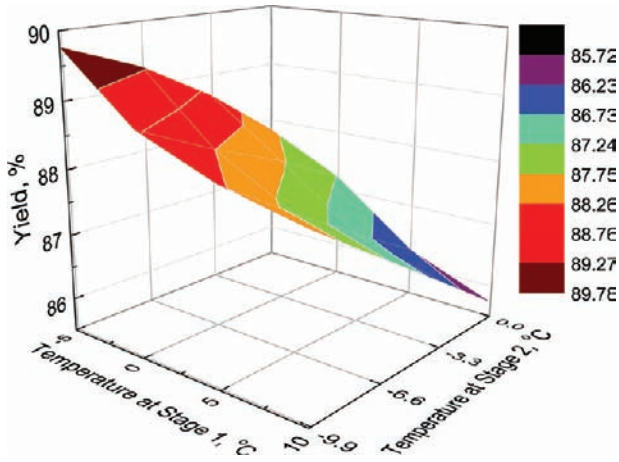

Figure 18. Effect of temperature at stages 1 and 2 on process yield.

Increasing the temperature even further would decrease the yield even more.

The effect of the temperature of each stage on the final crystal purity was also studied, and the results can be seen in Figure 19.

The results indicate that changing the temperatures of the stages results in a maximum purity difference of 0.7%. That is

dx.doi.org/10.1021/op2002886 | Org. Process Res. Dev. 2012, 16, 915−924

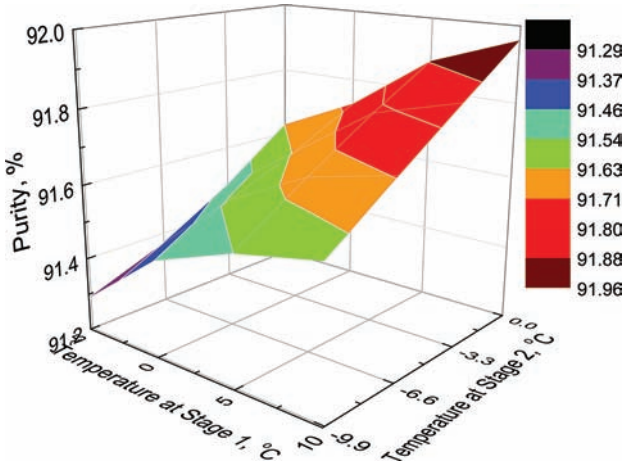

Figure 19. Effect of temperature at stages 1 and 2 on crystal purity.

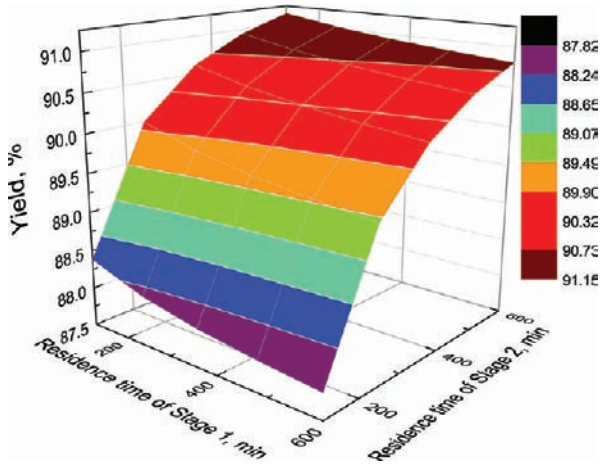

Figure 21. Effect of residence time at stage 1 and 2 on process yield.

because the entire process included both anti-solvent crystallization and cooling processes, and the influence of only temperature as shown here is not so significant. As the temperature in the second stage increases, the purity of the crystals also increases. This is due to the fact that, at steady state, the concentration of the impurities in the liquid phase in the second stage is reaching a higher level when the temperature is lower. The results from Figures 18 and 19 show that the temperatures at both of the two stages have opposite effects on purity and process yield. As process yield is increased, product purity decreases.

The influence of the residence time on the yield and purity of the final product were also evaluated as well, and the results are shown in Figures 20 and 21. The residence time of each stage

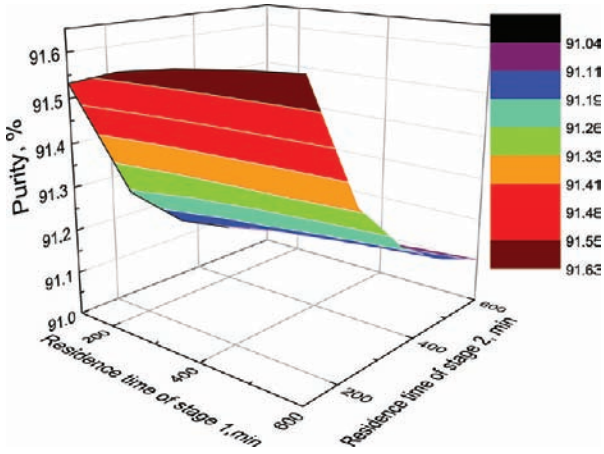

Figure 20. Effect of residence time at stage 1 and 2 on crystal purity.

was varied between 120 and 800 min. The product yield varied from 87.5% to 91.0%. The kinetics of crystal growth for Compound A are quite slow, so it takes a very long time for the concentration to reach the solubility limit. Not surprisingly, when the second stage had a very long residence time, the residence time of the first vessel did not affect the product yield significantly. For the product purity, the crystal purity decreased with increasing residence time. Increasing the residence time of the first vessel showed a greater effect on the purity than decreasing the residence time of the second vessel. The product purity ranged from 91.0% to 91.6%. Again, there was a negative correlation between product purity and yield when changing the residence time.

The relationship between the purity of the final product and the process yield has been correlated, and it can be clearly seen that there is an opposite influence of process parameters on the purity and yield. This behavior is shown in Figure 22.

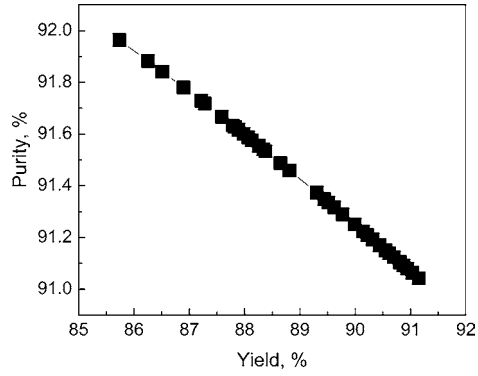

Figure 22. Purity of the crystals as a function of process yield for a continuous crystallization system.

The model was used to evaluate the effect of process parameters on the purity of the crystals and the process yield. The results of the model could be used to find out the optimal operating conditions to maximize yield without having too high impurity content.

Attributed to the growing interest in the development of continuous crystallization processes in the pharmaceutical industry, it has been an urgent requirement to develop robust continuous crystallization processes which produce API crystals with high yield and purity. While batch manufacturing process is still preferred in the current pharmaceutical industry, the development of continuous systems such as the one described in this paper will help the industry in moving from batch to continuous manufacturing.

4. CONCLUSIONS

A multistage cascaded MSMPR continuous crystallization system was optimized for the continuous crystallization of Compound A using cooling and anti-solvent to generate supersaturation. Its capability to crystallize an organic compound was experimentally demonstrated.

dx.doi.org/10.1021/op2002886 | Org. Process Res. Dev. 2012, 16, 915–924

XRD results indicate that the vessel in which anti-solvent is added has a significant influence on the final crystal properties. Adding anti-solvent in the second vessel resulted in crystals with increased crystallinity and better morphology for downstream processing. Focused beam reflectance measurement (FBRM) technology was employed to track the crystals size distribution of Compound A crystals.

A mathematical model was used to analyze the experimental results. By combining the process model with an optimization algorithm, the nucleation and growth rate parameters were extracted and used to predict the size distribution under different process conditions. The multistage MSMPR model was used to evaluate the effect of process conditions, including the temperature and residence time, on the purity of the crystal and the process yield in the continuous crystallization process of Compound A.

■ ASSOCIATED CONTENT

Supporting Information

Model equations used. This material is available free of charge via the Internet at http://pubs.acs.org.

■ AUTHOR INFORMATION

Corresponding Author

*E-mail: trout@mit.edu

Notes

The authors declare no competing financial interest.

■ ACKNOWLEDGMENTS

We acknowledge Novartis for funding and various supports.

■ NOTATION

Symbol Definition

b nucleation rate order [dimensionless]

g growth rate order [dimensionless]

k_b nucleation rate constant [number/m^3 min]

k_g crystal growth rate constant [m/s]

■ REFERENCES

(1) Myerson, A. S. *Handbook of Industrial Crystallization*, 2nd ed.; Butterworth-Heinemann: Boston, MA, 2002.

(2) Jones, A. G. *Crystallization Process Systems*; Butterworth-Heinemann: Oxford, UK, 2002.

(3) Mullin, J. W. *Crystallization*, 4th ed.; Butterworth-Heinemann: Oxford, UK, 2002.

(4) Randolph, A. D., Larson, M. A., *Theory of Particulate Process: Analysis and Techniques of Continuous Crystallization*, 2nd ed.; Academic Press: Toronto, Canada, 1988.

(5) Nyvlt, J. *Design of Crystallizers*; CRC Press: Boca Raton, FL, 1992.

(6) Nyvlt, J., *Solid-liquid equilibria*; Elsevier: Amsterdam, Holland, 1977.

(7) Chen, J.; Sarma, B.; Evans, J. M. B.; Myerson, A. S. *Cryst. Growth Des.* **2011**, *11*, 887−895.

(8) Tavare, N. S. *AIChE J.* **1986**, *32*, 705−732.

(9) Sheikh, A. Y.; Jones, A. G. *AIChE J.* **1998**, *44*, 1637−1645.

(10) Alvarez, A. J.; Myerson, A. S. *Cryst. Growth. Des.* **2010**, *10*, 2219−2228.

(11) Lawton, S.; Steele, G.; Shering, P.; Zhao, L. H.; Laird, I.; Ni, X. W. *Org. Process Res. Dev.* **2009**, *13*, 1357−1363.

(12) Hanley, T. R.; Mischike, R. A. *Ind. Eng. Chem. Fundam.* **1978**, *17*, 51−58.

(13) Trifkovic, M; Sheikhzadeh, M.; Rohani, S. *Ind. Eng. Chem. Res.* **2008**, *47*, 1586−1595.

(14) Ruf, A.; Worlitschek, J.; Mazzotti, M. *Part. Syst. Syst. Charact.* **2000**, *17*, 167−179.

(15) Nie, Q.; Wang, J.; Yin, Q. *Chem. Eng. Sci.* **2006**, *61*, 5962−5968.

(16) Sheikh, A. Y. *Modeling, Synthesis, Optimization and Control of Crystallization Processes*. PhD Thesis; University of London: London, 1997.

(17) Sheikh, A. Y.; Jones, A. G. *AIChE J.* **1997**, *43*, 1448−1457.

(18) Garside, J.; Jancic, S. J. *Chem. Eng. Sci.* **1978**, *33*, 1623−1630.

(19) Togkalidou, T.; Tung, H.-H.; Sun, Y.; Andrews, A.; Braatz, R. D. *Ind. Eng. Chem. Res.* **2004**, *43*, 6168−6181.

(20) Kempkes, M.; Eggers, J.; Mazzotti, M. *Chem. Eng. Sci.* **2008**, *63*, 4656−4675.

(21) Barrett, P.; Glennon, B. *Part. Part. Syst. Charact.* **1999**, *16*, 207−211.

(22) Tadayyon, A.; Sohrab Rohani, S. *Part. Part. Syst. Charact.* **1998**, *15*, 127−135.

(23) Ruf, A.; Worlitschek, J.; Mazzotti, M. *Part. Part. Syst. Charact.* **2000**, *17*, 167−179.

(24) Liu, W.; Clark, N. N.; Karamavruc, A. I. *Chem. Eng. Sci.* **1998**, *53*, 1267−1276.

(25) Hukkanen, J. E.; Braatz, D. R. *Sens. Actuators, B* **2003**, *96*, 451−459.

(26) Leyssens, T.; Baudry, C.; Hernandez, M. L. E. *Org. Process Res. Dev.* **2011**, *15*, 413−426.

(27) Nere, K. N.; Ramkrishna, D.; Parker, E. B.; Bell, V. W. III; Mohan, P. *Ind. Eng. Chem. Res.* **2007**, *46*, 3041−3047.